Numerical Evaluation of Displacement-Robust and Fault-Tolerant Four-Sensor Probe Arrays for Local Bubble Parameter Measurement in Two-Phase Flow

Minhong Cho, Xuan Quyet Do, Jinyeong Bak, Jae Jun Jeong, Byongjo Yun*
Department of Mechanical Engineering, Pusan National University, 2, 63 beon-gil, Busandaehak-ro, Geumjeong-gu, Busan 46241, Republic of Korea
**Corresponding author: bjyun@pusan.ac.kr*

Keywords : four-sensor probe, local bubble parameter, two-phase flow, bubble velocity,interfacial area concentration

1. Introduction

The conductance or optical fiber four-sensor probe is a widely used intrusive technique for the measurement of local two-phase flow parameters, such as void fraction, bubble velocity, interfacial area concentration (IAC) and Sauter mean diameter (D_{32}) measurement [1–5]. The accuracy of such IAC-based D_{32} measurements depends on both the selected IAC model [1-3] and the axial rear-sensor configuration, which governs the time-delay resolution and the geometric characteristics of the four-sensor probe. In addition, in high-pressure and high-temperature two-phase flow conditions, sensors may deform or fail during experiments, leading to sensor-tip displacement and signal loss, which can degrade measurement reliability. Most previous studies have adopted a conventional sensor configuration for a four-sensor probe comprising one front sensor and three coplanar rear sensors. However, this configuration becomes unusable if the front sensor fails, since the required front–rear time delays are no longer available. Therefore, the development of a new four-sensor probe array designed to address such situations is required.

This study aims to investigate the measurement performance of new four-sensor configurations for bubble parameters according to the axial distances between the three rear sensors using a Monte Carlo simulation [5]. A displacement robustness metric was introduced to quantify the sensitivity to axial sensor-tip displacement, and recovery strategies for single rear-sensor failure cases were examined. Based on the combined evaluation, an array-selection guideline was developed that accounts for measurement accuracy, displacement robustness, and fault handling.

2. Development of New 4-Sensor Configuration

2.1 Four-sensor configuration and measurement method

This study considers a four-sensor probe consisting of one front sensor (S_0) and three rear sensors (S_{1-3}) as shown in Fig. 1. The sensor layout on the *x*–*y* plane is fixed to a square, and candidate arrays are generated by varying only the axial rear-sensor spacings $\Delta z_k (k = 1,2,3)$. The reference axial spacing $z_{longest}$ is defined as the maximum of the three rear-sensor spacings, and the normalized axial spacings are defined as follows:

$$\Delta z_k' = n \frac{\Delta z_k}{z_{longest}}, k = 1,2,3 \quad (1)$$

where $\Delta z_k'$ denotes the discretized nondimensional axial spacing defined on an integer grid by dividing $z_{longest}$ into n equal segments. In this study, n is set to 4, and only arrays including at least one $\Delta z_k' = 4$ are evaluated so that all candidate arrays share the same $z_{longest}$ for fair comparison. This constraint yields a total of 37 candidate arrays. Array-to-array comparisons are performed based on $(\Delta z_1', \Delta z_2', \Delta z_3')$. In addition, arrays that make the denominator of the velocity-calculation equation equal to zero (e.g., $\Delta z_1 + \Delta z_3 = \Delta z_2$) are excluded, since the axial velocity cannot be computed in such cases.

Time delays Δt_k $(k = 1,2,3)$ are extracted from the bubble–sensor contact signals, and local bubble velocity is evaluated using an established four-sensor procedure that combines multi-sensor geometry with the time delays [4]. The axial component of the bubble velocity, V_{axial} is used as the primary velocity metric. Bubble size is quantified by the IAC-based D_{32}. IAC is obtained by applying established IAC models [1-3] to the locally measured void fraction (α) and velocity, and D_{32} is defined as follows:

$$D_{32} = \frac{6\alpha}{IAC} \quad (2)$$

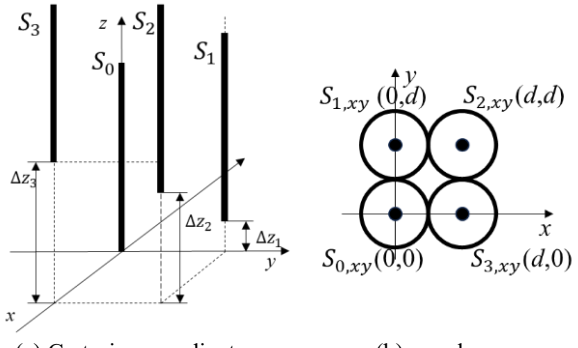

(a) Cartesian coordinates (b) *x*-*y* plane

Fig. 1. Four-sensor probe configuration

2.2 Monte Carlo simulation conditions and error metric

For each array, Monte Carlo simulations were performed by generating bubble events and computing V_{axial} and IAC-based D_{32} for each event. The bubble generation and calculation procedure follows Moon et al.

[5]. To ensure consistent array-to-array comparison under different axial spacings, the bubble size is normalized using the reference length $z_{longest}$:

$$D' \equiv \frac{D_{30}}{z_{longest}} \tag{3}$$

where D_{30} is the volume-equivalent spherical diameter. Bubble diameters were sampled from a normal distribution, and aspect ratios from a log-normal distribution to reflect statistical variability [5]. The imposed velocity fluctuation level is represented by the velocity fluctuation ratio:

$$H \equiv \frac{\Delta V}{V} \tag{4}$$

where ΔV denotes the magnitude of the imposed velocity fluctuation [5]. In the Monte Carlo simulation, H is uniformly sampled within $[0, H_{\max}]$. For consistent array comparison under typical experimental scales (V in m/s and sensor axial spacing in mm), a normalized velocity is defined as

$$V' \equiv \frac{V}{V_{ref}} \tag{5}$$

$$V_{ref} = 10^3 \frac{z_{longest}}{t_{ref}};\ t_{ref} = 1\ s \tag{6}$$

In the Monte Carlo simulation, the normalized velocity is fixed to $V' = 1.0$ to focus on sensor-spacing effects. In the present framework, changing V primarily rescales the time delays ($\Delta t \propto 1/V$) and does not affect the estimation error of computed quantities (V_{axial}, D_{32}) under the continuous-time assumption. In addition, V' is used only to define the simulation conditions, while the velocity used in the event-wise calculations follows the original formulation [4]. The Monte Carlo simulation conditions are summarized as follows:

- D' range: 0.1–5.0, binned into $N_{\text{case}} = 50$ cases
- $N_b = 250{,}000$ bubbles per case
- $H_{max} = 0.0, 0.2$
- $V' = 1.0$

Prediction accuracy was quantified using mean absolute percentage error (MAPE), and the results of $H_{\max} = 0.0\ and\ 0.2$ were combined with equal weighting.

2.3 Displacement robustness and sensor-fault correction

To emulate practical uncertainties, small axial displacement δ is imposed on the rear-sensor tip positions ($k = 1,2,3$). From a first-order sensitivity analysis of the four-sensor V_{axial} formulation, the displacement sensitivity index (K) is expressed as follows:

$$|\ K\ | = \frac{1}{|\Delta z_1 - \Delta z_2 + \Delta z_3|} \tag{7}$$

Since $\Delta z_k'$ scales with Δz_k, a larger $|\ \Delta z_1' - \Delta z_2' + \Delta z_3'\ |$ implies lower displacement sensitivity and a more robust array.

A single rear-sensor fault scenario is considered ($S_{\text{fault}} = 1,2,3$), where one of the three rear sensors becomes unavailable. Three strategies are evaluated: (i) two-sensor fallback [3]; (ii) interpolation method, which reconstructs the missing time delay $\Delta t_{k,\text{missing}}$ by assuming a linear proportionality between Δt_k and Euclidean distance s_k for each front-rear sensor pair, using Eq. (8); and (iii) analytical method, which estimates $\Delta t_{k,\text{missing}}$ using the functional form of the four-sensor axial-velocity equation together with the array geometry, using Eq. (9).

$$\Delta t_{c,missing}^{interp} = \Delta t_a + (s_c - s_a)\frac{\Delta t_b - \Delta t_a}{s_b - s_a} \tag{8}$$

$$\Delta t_{1,missing}^{ana} = \frac{(\Delta z_1 - \Delta z_2 + \Delta z_3)}{V_{axial}} + \Delta t_2 - \Delta t_3 \tag{9a}$$

$$\Delta t_{2,missing}^{ana} = -\frac{(\Delta z_1 - \Delta z_2 + \Delta z_3)}{V_{axial}} + \Delta t_1 + \Delta t_3 \tag{9b}$$

$$\Delta t_{3,missing}^{ana} = \frac{(\Delta z_1 - \Delta z_2 + \Delta z_3)}{V_{axial}} + \Delta t_2 - \Delta t_1 \tag{9c}$$

where *a* and *b* denote the available front–rear pairs and *c* denotes the missing pair. Here, $\Delta z_k'$ is used only for normalized array-to-array comparison, while Δz_k denotes the physical axial spacings used in Eq. (9).

3. Results

3.1 Evaluation results of V_{axial} and D_{32} measurements

Figure 2 summarizes the MAPE of the axial velocity V_{axial} for candidate arrays under two representative velocity-fluctuation conditions ($H_{\max} = 0.0$ and 0.2). For $H_{\max} = 0.0$, the error generally decreases as $\Delta z_1'$, $\Delta z_2'$, and $\Delta z_3'$ increase, and the conventional configuration, V-1 $(\Delta z_1', \Delta z_2', \Delta z_3')$=(4,4,4) array yields the minimum MAPE of 0.03%. For $H_{\max} = 0.2$, the error decreases with increasing $\Delta z_1'$ and decreasing $\Delta z_2'$, while the dependence on $\Delta z_3'$ is less pronounced; however, for $\Delta z_2' = 1$, larger $\Delta z_3'$ leads to a lower error. Consequently, the V-2 (4,1,4) array provides the best performance with a minimum MAPE of 0.08% under $H_{\max} = 0.2$.

Table I summarizes the best-performing arrays for IAC-based D_{32} measurement using the three IAC models. The Kataoka et al. [1] and Revankar & Ishii [2] models show significantly larger minimum errors (MAPE = 85.25% and 25.07%, respectively) compared to the Le Corre & Ishii (LC) [3] model, which achieves approximately 4% MAPE. Therefore, subsequent analyses are primarily based on the LC model. For the LC model, no clear trend with respect to $\Delta z_k'$ is observed. However, arrays including $\Delta z_k' = 1$ tend to yield relatively smaller errors.

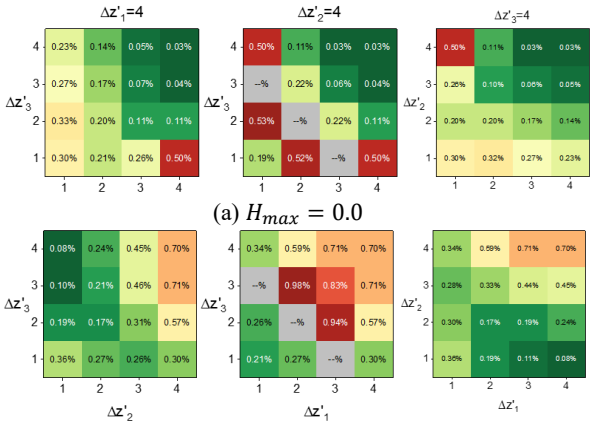

(a) $H_{max} = 0.0$

(b) $H_{max} = 0.2$

Fig. 2. MAPE of V_{axial}

Table I: MAPE of D_{32}

IAC Model	Array	$\Delta z_1'$	$\Delta z_2'$	$\Delta z_3'$	MAPE [%]
Kataoka et al. [1]	K-1	2	4	3	85.25
Revankar & Ishii [2]	R-1	2	4	3	25.07
Le Corre & Ishii [3]	LC-1	2	1	4	4.04
	LC-2	4	1	3	4.25

3.2 Evaluation of displacement robustness

To assess displacement robustness, an axial perturbation of magnitude $\delta = 0.1\, z_{longest}$ is imposed on the rear-sensor tip positions under the same Monte Carlo conditions defined in Section 2.2. Three representative arrays are selected for comparison: the conventional array V-1 (4,4,4), the most sensitive array K-1 (2,4,3) with the minimum $|\Delta z_1' - \Delta z_2' + \Delta z_3'|$, and the most robust array among the representative arrays V-2 (4,1,4) with the maximum $|\Delta z_1' - \Delta z_2' + \Delta z_3'|$.

Fig. 3 presents the displacement-induced error in V_{axial}, and Fig. 4 presents the corresponding error in IAC-based D_{32} (LC model), for a representative case where a displacement ($+\delta$) is applied to rear sensor 1. In both figures, the same trend is observed: the error decreases as $|\Delta z_1' - \Delta z_2' + \Delta z_3'|$ increases, supporting the use of this quantity as a displacement robustness metric. The velocity error remains nearly constant over the entire D' range, whereas the D_{32} error increases as D' decreases.

For an unbiased comparison, Table II reports the overall MAPE averaged over rear sensor index $k = 1$–3, both displacement directions ($\pm\delta$), and the full diameter range of D', for V_{axial} and IAC-based D_{32}. The consistent ranking among V-2, V-1, and K-1 further supports $|\Delta z_1' - \Delta z_2' + \Delta z_3'|$ as a selection metric for arrays robust to displacement.

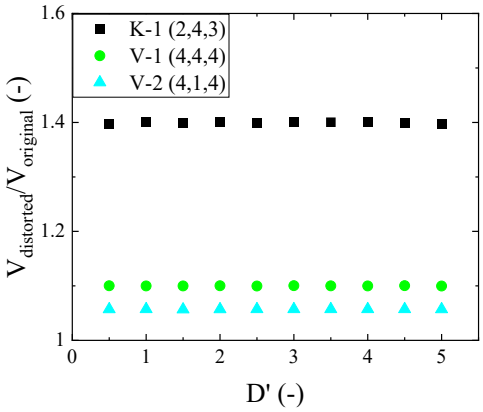

Fig. 3. Displacement effect on V_{axial} measurement

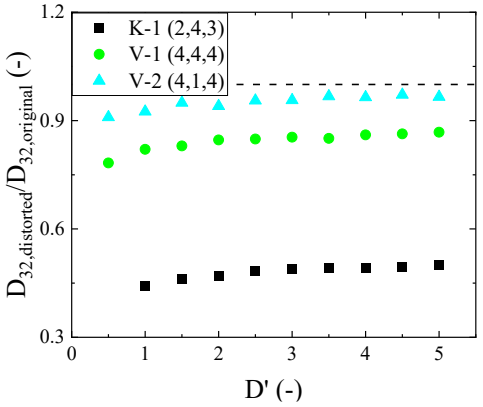

Fig. 4. Displacement effect on D_{32} measurement

Table II: Displacement-induced MAPE

Array	$\lvert\Delta z'_1\text{-}\Delta z'_2\text{+}\Delta z'_3\rvert$	V_{axial}	D_{32} (LC)
K-1 (2,4,3)	1	40.00 %	26.38 %
V-1 (4,4,4)	4	10.00 %	7.12 %
V-2 (4,1,4)	7	5.71 %	3.52 %

Based on the combined results of Sections 3.1 and 3.2, LC-2 (4,1,3) is selected as the recommended array by considering measurement accuracy, displacement robustness, and practical fault tolerance. Specifically, LC-2 achieves a low MAPE of 4.25% for D_{32} using the LC model and provides accurate V_{axial} measurements with a MAPE of 0.19%. In addition, LC-2 has $|\Delta z_1' - \Delta z_2' + \Delta z_3'| = 6$, indicating reduced displacement sensitivity compared to the conventional array (V-1). Moreover, the distinct rear-sensor elevations maintain usability under rear-sensor faults, using the proposed correction methods for single-sensor failure and the two-sensor fallback for double-sensor failure.

3.3 Evaluation of sensor-fault correction methods

Table III compares three correction methods for the recommended array LC-2 by reporting the mean MAPE of V_{axial} and IAC-based D_{32} (LC model), averaged over the single rear-sensor fault cases ($S_{\text{fault}} = 1$–3) and the full D' range. For both V_{axial} and D_{32}, the analytical method yields the lowest MAPE, outperforming the two-sensor fallback and the interpolation method. Therefore, the analytical method is recommended as the primary correction strategy for maintaining both V_{axial} and D_{32} measurement accuracy under a single rear-sensor failure.

Table III: Evaluation results of correction methods

Method	V_{axial}	D_{32} (LC model)
2-sensor	2.57 %	13.99 %
Interpolation	8.34 %	18.14 %
Analytical	1.72 %	10.28 %

4. Conclusions

The performance of a four-sensor probe was evaluated by systematically varying the generalized rear-sensor axial-spacing configuration under a normalized representation and quantifying the resulting MAPE in V_{axial} and IAC-based D_{32} using Monte Carlo simulations. Based on the evaluation results, representative arrays were selected for V_{axial} and D_{32} measurement. Displacement robustness was then assessed using the displacement robustness metric $|\Delta z_1' - \Delta z_2' + \Delta z_3'|$, and the simulation results confirmed that increasing this metric reduces the sensitivity of the V_{axial} and D_{32} to axial sensor-tip displacement. Accordingly, LC-2 (4,1,3) is recommended as a practically implementable array, as it achieves low measurement error with reduced displacement sensitivity and remains applicable under sensor-fault conditions. Finally, three correction strategies for single rear-sensor failure—two-sensor fallback, interpolation, and analytical methods—were formulated and evaluated, and the analytical method yielded the smallest errors for both V_{axial} and D_{32}.

NOMENCLATURE

D_{30}	Volume-equivalent spherical diameter (mm)
D_{32}	Sauter mean diameter (mm)
D'	Normalized bubble diameter (–)
H_{max}	Maximum velocity fluctuation ratio (–)
N_{case}	Number of cases (–)
N_b	Number of bubbles (–)
s	3-D distance between front-rear sensors (mm)
S	Sensor
t	Time (s)
V_{axial}	Axial bubble velocity (m/s)
x, y, z	Cartesian coordinates (mm)
$z_{longest}$	Longest axial sensor spacing (mm)

Greek symbols

α	Local void fraction (-)
Δt_k	Time delay between front-rear sensor k (s)
$\Delta z_k'$	Normalized axial spacing (–)
δ	Axial displacement magnitude (mm)

Subscripts

k	Sensor index (k =0, 1, 2, 3)
avg	Averaged value
cal	Calculated value
ref	Reference value
original	Value without displacement
distorted	Value with displacement
missing	Missing value due to sensor-fault

Superscripts

$'$	Normalized parameter

ACKNOWLEDGEMENT

This work was supported by the National Research Foundation of Korea (NRF) grant funded by the Korea government (MSIT) (No. RS-2023-00257680) and by the Korea Institute of Energy Technology Evaluation and Planning (KETEP) and the Ministry of Climate, Energy & Environment (MCEE) of the Republic of Korea (20222B10100110).

REFERENCES

[1] I. Kataoka, M. Ishii, and A. Serizawa, “Local formulation and measurements of interfacial area concentration in two-phase flow”, *Int. J. Multiphase Flow*, vol. 12, no. 4, pp. 505–529, 1986, https://doi.org/10.1016/0301-9322(86)90057-1.

[2] S. T. Revankar and M. Ishii, “Theory and measurement of local interfacial area using a four sensor probe in two-phase flow”, *Int. J. Heat Mass Transf.*, vol. 36, no. 12, pp. 2997–3007, 1993, https://doi.org/10.1016/0017-9310(93)90029-6.

[3] J. M. Le Corre and M. Ishii, “Numerical evaluation and correction method for multi-sensor probe measurement techniques in two-phase bubbly flow”, *Nucl. Eng. Des.*, vol. 216, no. 1–3, pp. 221–238, 2002, https://doi.org/10.1016/S0029-5493(02)00130-9.

[4] X. Shen, Y. Saito, K. Mishima, H. Nakamura, “Methodological improvement of an intrusive four-sensor probe for the multi-dimensional two-phase flow measurement”, *Int. J. Multiphase Flow*, vol. 31, no. 5, pp. 593–617, 2005, https://doi.org/10.1016/j.ijmultiphaseflow.2005.02.003.

[5] J. Moon, Y. Ko, S. G. Nam, J. J. Jeong, B. Yun, "Evaluation of the multi-sensor probe methods for the measurement of local bubble velocity and diameter", *Int. Commun. Heat Mass Transf.*, vol. 135, 106146, 2022, https://doi.org/10.1016/j.icheatmasstransfer.2022.106146.